

# Research Letter

# Optical thermal insulation via the photothermal effects of Fe<sub>3</sub>O<sub>4</sub> and Fe<sub>3</sub>O<sub>4</sub>@Cu<sub>2-x</sub>S thin films for energy-efficient single-pane windows

Jou Lin, Yuan Zhao, and Donglu Shi, The Materials Science and Engineering Program, Department of Mechanical and Materials Engineering, College of Engineering and Applied Science, University of Cincinnati, Cincinnati, OH 45221, USA

Address all correspondence to Donglu Shi at shid@ucmail.uc.edu

(Received 11 November 2019; accepted 2 January 2020)

#### **Abstract**

To address critical energy issues in civic structures, we have developed a novel concept of optical thermal insulation (OTI) without relying on a conventional thermal intervention medium, such as air or argon, as often used in conventional window systems. We have synthesized the photothermal (PT) materials, such as the  $Fe_3O_4$  and  $Fe_3O_4$ @ $Cu_{2-x}S$  nanoparticles, that exhibit strong UV and near-infrared (NIR) absorptions but with good visible transparency. Upon coating the inner surface of the window glass with a PT film, under solar irradiation, the inner surface temperature rises due to the PT effect. Subsequently, the temperature difference,  $\Delta T$ , is reduced between the single pane and room interior. This leads to lower the thermal loss through a window, reflected by the U-factor, resulting in considerable energy saving without double- or triple-glazing. Comparing with the  $Fe_3O_4$  coatings,  $Fe_3O_4$ @ $Cu_{2-x}S$  is spectrally characterized with a much stronger NIR absorbance, contributing to an increased PT efficiency under simulated solar irradiation (0.1 W/cm²). PT experiments are carried out via both white light and monochromic NIR irradiations (785 nm). The parameters associated with the thermal performance of the PT films are calculated, including PT conversion efficiency, specific absorption rate (SAR), and U-factor. Based on the concept of OTI, we have reached an optimum U-factor of 1.46 W/m² K for a single pane, which is satisfactory to the DOE requirement (<1.7 W/m² K).

#### Introduction

Thermal insulation has been a great challenge in energy saving particularly for commercial buildings in cold climate. Conventional buildings are commonly structured with windows enframed within the building walls that compromise between lighting and heat transfer. One of the key issues deals with overall building energy and material consumptions, including electricity, heating, and cooling, and materials production simply due to their large sheer sizes. A new trend in architecture has been transforming traditional windows to glazed building façade with finesse that almost entirely covers the building surface areas. However, great challenges remain in terms of thermal transfer, energy efficiency, and lighting requirements, especially heat loss in cold climate. Although various technologies have been developed to improve thermal transmittance, including low emissivity coating and double/triple panes, huge consumption of energy will not be resolved until fundamentally different new concepts and engineering innovations are developed. The U.S. Energy Information Annual (EIA) reported 5.3 quadrillion British thermal units (quad) energy consumptions of primary heat loss from ventilation, heating, and air conditioning system in 2018 in the USA.[1]

The US Advanced Research Projects Agency – Energy (ARPA-E) initiated a program on replacing double-pane windows with single panes for improving energy and materials

consumptions of commercial buildings especially for cold climate regions. [2] The overall heat transfer coefficient: U-factor is a measure of heat loss by conduction, radiation, and convection. [3] A lower *U*-factor indicates a higher thermal insulation or lower energy transfer through a window. To lower the U-factor, the conventional approach has been replying on a thermal insulation medium, such as air or argon, that requires the glazing technologies. However, only a few insulation materials currently available that are not only highly thermally insulating but also significantly transparent for window applications. We demonstrate a novel concept of optical thermal insulation (OTI) without any intervening medium. Instead of applying a thermal insulator, a transparent photothermal (PT) film can selectively absorb photons in the UV and near-infrared (NIR) regions and efficiently convert them to heat, therefore raising the building skin surface temperature (via free energy). As the inner building skin temperature is raised relative to room temperature, the heat transfer at the building skin inner surface can be effectively reduced via OTI, characterized by a low *U*-factor. The solar spectrum can be divided into three primary regions, including ultraviolet (below 400 nm), visible (400-700 nm), and infrared light (above 700 nm). According to the standard solar radiation spectra, [4] there are approximately 49% of heat provided by infrared light. The critical requirements of OTI are: (i) it is highly transparent but only absorbing UV and NIR for energy conversion



and (ii) upon absorbing solar light in the UV and NIR regions, energy conversion is efficient and able to effectively raise the window inner surface temperature for the reduction of the *U*-factors. These requirements are spectrally characterized with a "U"-shaped absorption, i.e., high UV and NIR absorptions, but low absorptions in the visible band.

The PT effect is characterized by the absorption of electromagnetic radiation in a particular wavelength and conversion to thermal energy within a short period of time. The PT effect has been extensively and primarily studied for medical treatment. [5-10] Most of the PT materials applied for medical therapeutics mainly focused on noble metals, [5,11,12] carbon-based materials, [6] and metal oxide composites. [7-9,13] Although metallic materials exhibit strong PT responses upon NIR light irradiation, none is qualified for OTI due to their nontransparent nature. Note that, in all previous studies, the PT nanoparticles were only synthesized in extremely small quantities in milligrams and applied in the aqueous solutions. Zhao et al., for the first time, deposited a thin coating of Fe<sub>3</sub>O<sub>4</sub> nanoparticles on a glass substrate for window applications and found the film not only quite transparent with significant average visible transmittance (AVT) but also efficiently PT resulting in very low U-factors even below those of the double panes, therefore making single pane highly possible.<sup>[13]</sup> However, the absorption of Fe<sub>3</sub>O<sub>4</sub> is majorly focused near UV, but rapidly decreasing and diminishing in the NIR range. As noted above, the key to enhancing the PT effect is to have both strong UV and NIR absorptions forming a "U"-shaped spectrum with high AVT.

Tian et al. reported a core-shell nanoparticle suspension solution of Fe<sub>3</sub>O<sub>4</sub>@Cu<sub>2-x</sub>S that exhibits an absorption peak at 960 nm in UV-Vis-NIR absorption spectra, providing a unique PT characteristic that is lacking in the Fe<sub>3</sub>O<sub>4</sub> system.<sup>[9]</sup> The Cu<sub>2-x</sub>S nanocrystal has a tunable localized surface plasmon resonance (LSPR) in the NIR region.[10] Several studies investigated the energy conversion mechanisms of CuS and gold nanoparticles based on LSPR.[10-12,14] Compared to surface plasmon resonance (SPR), LSPR is related to size, shape, and surrounding materials of the nanoparticles. [15] A nanoparticle's response to the oscillating electric field can be described by the dipole approximation of Mie scattering theory[11,14] based on which the extinction efficiency of Fe<sub>3</sub>O<sub>4</sub> has been calculated. [16] Specifically, Mie scattering applies to the condition where the size of the scattering particle is comparable to the wavelength of the incident light.<sup>[17]</sup> Wei et al. showed that LSPR of Cu<sub>2-x</sub>S originates from the concentration of holes being reduced by the copper vacancies in copper chalcogenides nanocrystals. [14] Hence, the PT effect can be affected by the nanoparticle size, shape, and dielectric constant.

In this study, we investigated the PT effects of thin films of both  $Fe_3O_4$  and  $Fe_3O_4@Cu_{2-x}S$  irradiated by simulated solar light (0.1 W/cm²) and monochromic irradiation (785 nm laser, 0.1 W/cm²).  $Fe_3O_4$  and  $Fe_3O_4@Cu_{2-x}S$  nanoparticles were synthesized by the one-pot synthesis, and their thin films were deposited by spin-coating for single-pane window applications. The PT effects of the thin films were investigated

based on the absorption spectra and Raman scattering. The correlations between the *U*-factor and visible transmittance were established for both Fe<sub>3</sub>O<sub>4</sub> and Fe<sub>3</sub>O<sub>4</sub>@Cu<sub>2-x</sub>S films.

## **Experimental details**

The chemicals of this research including iron (III) acetylacetonate (Fe(acac)<sub>3</sub>, ≥99.9%), copper (II) acetylacetonate (Cu (acac)<sub>2</sub>, ≥99.9%), oleylamine (70%), sulfur (99.998%), *N*-methyl-2-pyrrolidone (99.5%), and chloroform (≥99.9%) were purchased from Sigma-Aldrich Inc. (Milwaukee, WI, USA). Cyclohexane was purchased from Tedia Inc. (Fairfield, OH, USA). Poly (methyl methacrylate) was purchased from Polysciences Inc. (Warrington, PA, USA).

Fe<sub>3</sub>O<sub>4</sub> and Fe<sub>3</sub>O<sub>4</sub>@Cu<sub>2-x</sub>S nanoparticles were synthesized by a modified procedure from the literature. <sup>[9]</sup> Specifically, 90 mL of oleylamine was heated to 300 °C in a three-necked flask and stirred for 30 min in a nitrogen environment. Subsequently, a solution containing 18 mL of oleylamine, 12 mL of *N*-methyl-2-pyrrolidone, and 2.12 g of Fe(acac)<sub>3</sub> was injected into the flask. After keeping at 300 °C for 10 min, slowly cooled down to 60 °C for 10 min. When the Fe<sub>3</sub>O<sub>4</sub> solution was cooled down to room temperature, the nanoparticles were collected by a strong magnet and washed three times with methanol. The collected nanoparticles were freeze-dried (Labconco corporation). After drying, the Fe<sub>3</sub>O<sub>4</sub> nanoparticles were dispersed in toluene for later use.

For synthesizing the Fe<sub>3</sub>O<sub>4</sub>@Cu<sub>2-x</sub>S nanoparticles, 60 mL of oleylamine was heated to 300 °C in a three-necked flask and stirred for 30 min in a nitrogen environment. Subsequently, injecting a solution containing 12 mL of oleylamine, 8 mL of N-methyl-2-pyrrolidone, and 700 mg of Fe (acac)<sub>3</sub> into the flask. Keeping the solution at 300 °C for 10 min, it was then cooled down to 70 °C for 10 min. 128.28 mg of sulfur dissolved in 12 mL of oleylamine was mixed with 10 mL of cyclohexane and injected into the previous solution. After stirring at 70 °C for 10 min. 523.52 mg of Cu (acac)<sub>2</sub> dissolved in 4 mL of oleylamine and 16 mL of chloroform solution was injected into the solution. The final mixture was kept at 70 °C and stirred for 30 min. The Fe<sub>3</sub>O<sub>4</sub>@Cu<sub>2-x</sub>S nanoparticles were collected by a strong magnet and washed three times with methanol, and then freeze-dried. After drying, nanoparticles were dispersed in toluene for later use.

To prepare the thin-film samples,  $2.54 \times 2.54$  cm<sup>2</sup> micro slides were sonicated in acetone for 15 min, subsequently sonicated in isopropyl alcohol for another 15 min, and dried at 50 °C for 30 min in an isotemp oven 500 series (Fisher Scientific). Toluene solutions containing various concentrations of Fe<sub>3</sub>O<sub>4</sub> and Fe<sub>3</sub>O<sub>4</sub>@Cu<sub>2-x</sub>S nanoparticles were fixed with 5% PMMA. The solutions were spin-coated on glass substrates for 10 s at 1000 rpm. Each glass slide was coated with 80  $\mu$ L solution.

For PT experiments, samples were irradiated by 0.1 W/cm<sup>2</sup> white light using the Newport 150 W solar simulator (Lamp model 67005) and by 0.1 W/cm<sup>2</sup>, 785 nm laser (SFOLT Co., Ltd). The temperature was measured and recorded by using

an infrared camera (FLIR E6). A black sheet was placed under the sample to avoid reflection of light. The power density of solar simulator was calibrated by an optical power meter (Coherent Inc.). There were two main steps in this experiment, namely heating and cooling. Nanoparticle size was determined by transmission electron microscopy (TEM). The absorption and transmittance spectra were obtained by a UV–VIS NIR spectrometer Lambda 900 (PerkinElmer Inc.). The AVT was measured by a light transmittance meter (LS116, Linshang, Co. Ltd.). The Raman spectra were acquired by Raman spectroscopy excited by both 514 and 785 nm He–Ne lasers (Renishaw inVia).

The power densities on the samples from the solar simulator and 785 nm laser were both 0.1 W/cm<sup>2</sup>. An infrared camera was employed to measure the temperature of the samples. For heating curves, temperatures were recorded every min for the first 10 min. After 10 min, the light source was turned off. After turning off the light source, the cooling curve was determined by recording the temperature for 5 min.

The change in temperature increase is the key factor in the PT effect. However, in PT testing, the temperatures of heating and cooling are relative due to the solar simulator not only heating the sample but also raising the environment temperature. Consequently, the temperature data plotted are relative temperature changes. The relative temperature change (or change in temperature increase) can be obtained by using the following equations:

$$T_{S.0} - T_{Ref.0} = T_0 \tag{1}$$

$$(T_{S,x} - T_{Ref,x}) - T_0 = \Delta T$$
 (2)

where  $T_{\rm S,0}$  and  $T_{\rm R,0}$  are, respectively, the initial sample temperature and the initial environment temperature without irradiation;  $T_{\rm S,x}$  and  $T_{\rm R,x}$  are the sample temperature and the environment temperature under light irradiation; and  $\Delta T$  is the change in temperature increase.

### **Results and discussion**

 $Fe_3O_4^{[13]}$  and  $Fe_3O_4@Cu_{2-x}S^{[9]}$  nanoparticles were synthesized respectively by modified procedures based on the previously published reports. Figure 1(a) shows the change in temperature increase as a function of time for the Fe<sub>3</sub>O<sub>4</sub> thin films of various concentrations irradiated by white light (i.e., simulated solar light). Expectedly, AVT decreases as the concentration increases, resulting in a linear relationship between the maximum temperature increase,  $\Delta T_{\rm max}$  [the highest point from each heating curve in Fig. 1(a)], and AVT, as shown in Fig. 1(b). Note that in Fig. 1(b), each AVT point respectively corresponds to a concentration, accordingly: 65%, 70%, 75%, 80%, 85%, and 91% with the highest AVT (91%) for the glass substrate. The PT effects of these Fe<sub>3</sub>O<sub>4</sub> thin films irradiated by the 785 nm laser are shown in Fig. 1(c). As shown in this figure, there are less temperature increases compared to those irradiated by the white light [Fig. 1(a)]. A similar linear relationship between  $\Delta T_{\rm max}$  and AVT is shown in Fig. 1(d) for the 785 nm laser irradiated samples. Comparing both irradiations for the highest concentration of  $4.57 \times 10^{-4}$  g/cm<sup>2</sup>, one can see that the maximum temperature increase reaches 6.53 °C under simulated solar, while that is only 5.10 °C under the 785 nm laser irradiation.

Figure 1(e) shows the change in temperature increase,  $\Delta T$ , as a function of time for the Fe<sub>3</sub>O<sub>4</sub>@Cu<sub>2-x</sub>S thin films of various concentrations irradiated by white light (i.e., simulated solar light). In a similar fashion, AVT is inversely proportional to concentration. For instance, the AVT is only 65% for the highest Fe<sub>3</sub>O<sub>4</sub>@Cu<sub>2-x</sub>S concentration of  $5.08 \times 10^{-4}$  g/cm<sup>2</sup>, as shown in Fig. 1(f). A linear relationship is also found between  $\Delta T_{\rm max}$  and AVT for the Fe<sub>3</sub>O<sub>4</sub>@Cu<sub>2-x</sub>S thin films [Fig. 1(f)]. The heating curves by the 785 nm laser irradiation are shown in Fig. 1(g). As shown in this figure,  $\Delta T_{\rm max}$  reaches 7.77 °C under 785 nm laser irradiation, considerably higher than that by simulated solar irradiation (7.10 °C). The corresponding linear relationship between  $\Delta T_{\rm max}$  and AVT is shown in Fig. 1(h) for Fe<sub>3</sub>O<sub>4</sub>@Cu<sub>2-x</sub>S samples by the 785 nm laser irradiation.

Figures 2(a) and 2(b) show the UV–Vis/NIR transmittance and absorption spectra of the Fe<sub>3</sub>O<sub>4</sub> thin films of various concentrations. As shown in Fig. 2(a), the Fe<sub>3</sub>O<sub>4</sub> thin films exhibit strong absorption near the UV region and rapidly decrease in the visible region. Only weak absorption is observed in the NIR regions. Correspondingly, as shown in Fig. 2(b), the films retain considerable AVTs in the visible region, providing significant transparency. This is consistent with the heating curves shown in Fig. 1(a) that the white light irradiation generates more heat for a greater increase in temperature for a wider band of absorption in the visible region. In contrast, the temperature increase is not as significant by the 785 nm laser for much less absorption in the NIR region.

A quite different absorption and transmittance spectra were observed for the Fe<sub>3</sub>O<sub>4</sub>@Cu<sub>2-x</sub>S thin films as shown in Figs. 2(c) and 2(d). As shown in Fig. 2(c), the Fe<sub>3</sub>O<sub>4</sub>@Cu<sub>2-x</sub>S thin films exhibit much stronger absorption in a wide range of NIR extending up to 1400 nm for all concentrations investigated. An interesting characteristic of the absorption is the "U"-shaped curve for all concentrations with a minimum within the visible range. This is a particularly important feature for window applications. As mentioned above, one of the key requirements is to have strong UV and NIR absorptions, but minimum absorption in the visible region for high AVTs. As a result, the AVT of the Fe<sub>3</sub>O<sub>4</sub>@Cu<sub>2-x</sub>S thin film is rather substantial reaching even 90% for the concentration of  $3.55 \times 10^{-4}$  g/cm<sup>2</sup> in the visible region [Fig. 2(d)]. These spectra data are also consistent with the heating curves shown in Figs. 1(e) and 1(g) that the temperature increases are comparable when irradiated by either the white light or the 785 nm laser for its pronounced absorption in the NIR region.

As LSPR can be affected by inter-particle interactions, we also investigated the absorption behavior of the Fe<sub>3</sub>O<sub>4</sub> and Fe<sub>3</sub>O<sub>4</sub>@Cu<sub>2-x</sub>S nanoparticles dispersed in toluene by UV–Vis–NIR spectroscopy. Figure 3(a) shows the absorption

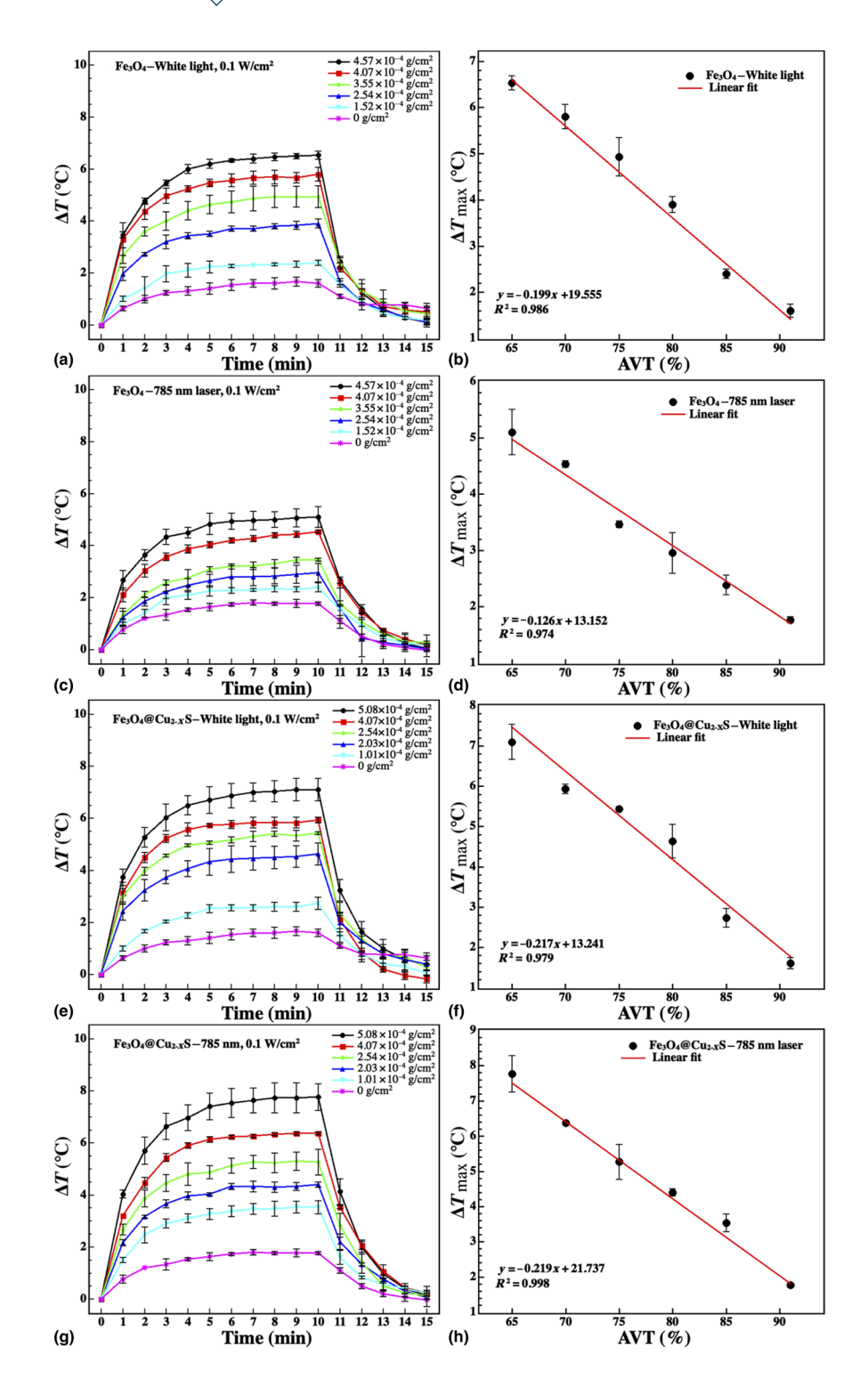


Figure 1. (a) The change in temperature increase,  $\Delta T$ , versus time curves under white light irradiation for the Fe<sub>3</sub>O<sub>4</sub> thin films of different concentrations. (b) The maximum change in temperature increase,  $\Delta T_{\text{max}}$ , versus AVT for the Fe<sub>3</sub>O<sub>4</sub> thin films of different concentrations under white light irradiation. (c) The change in temperature increase,  $\Delta T_{\text{max}}$ , versus time curves under the 785 nm laser irradiation for the Fe<sub>3</sub>O<sub>4</sub> thin films of different concentrations. (d) The maximum change in temperature increase,  $\Delta T_{\text{max}}$ , versus AVT for the Fe<sub>3</sub>O<sub>4</sub> thin films of different concentrations under the 785 nm laser irradiation. (e) The change in temperature increase,  $\Delta T_{\text{max}}$ , versus time curves under white light irradiation for the Fe<sub>3</sub>O<sub>4</sub>@Cu<sub>2-x</sub>S thin films of different concentrations. (f) The maximum change in temperature increase,  $\Delta T_{\text{max}}$ , versus time curves under the 785 nm laser irradiation for the Fe<sub>3</sub>O<sub>4</sub>@Cu<sub>2-x</sub>S thin films of different concentrations. (h) The maximum change in temperature increase,  $\Delta T_{\text{max}}$ , versus AVT for the Fe<sub>3</sub>O<sub>4</sub>@Cu<sub>2-x</sub>S thin films of different concentrations. (h) The maximum change in temperature increase,  $\Delta T_{\text{max}}$ , versus AVT for the Fe<sub>3</sub>O<sub>4</sub>@Cu<sub>2-x</sub>S thin films of different concentrations. Intensities of the white light and 785 nm laser are both 0.1 W/cm<sup>2</sup>. The environment temperature is 25 °C.

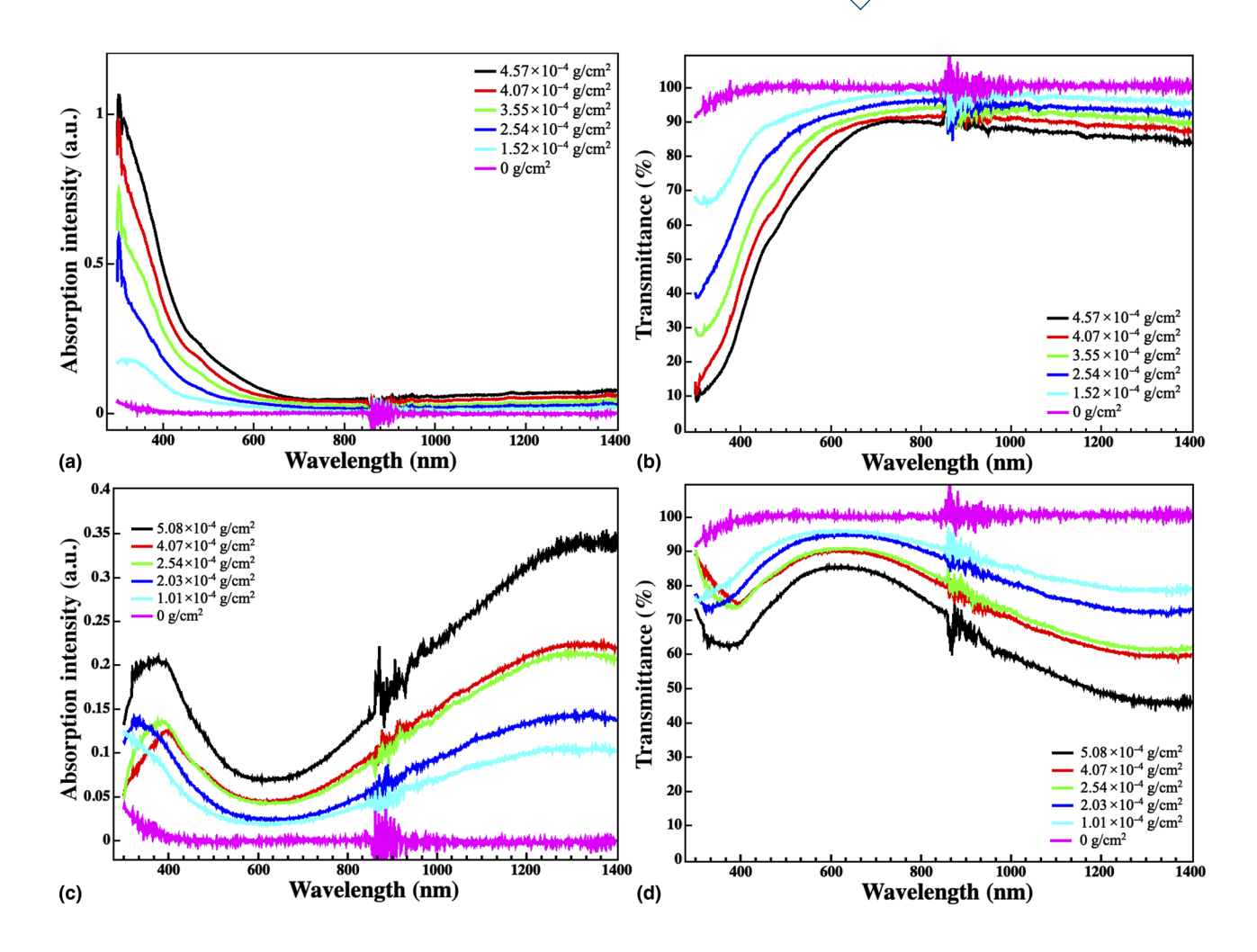


Figure 2. (a) Absorption and (b) transmittance spectra of the  $Fe_3O_4$  thin films of various concentrations. (c) Absorption and (d) transmittance spectra of the  $Fe_3O_4@Cu_{2-x}S$  thin films of various concentrations.

spectra of the Fe<sub>3</sub>O<sub>4</sub> and Fe<sub>3</sub>O<sub>4</sub>@Cu<sub>2-x</sub>S suspensions with the same concentration. As shown in this figure, the Fe<sub>3</sub>O<sub>4</sub>@Cu<sub>2-x</sub>S solution has an absorption peak at 1160 nm considerably shorter than that of the thin film counterpart (1349 nm), indicating particle interaction dependent absorption. Interestingly, the minimum of the "U"-shaped curve is also shifted from 639 nm for the thin film to 560 nm for the solution. The absorption behaviors of both Fe<sub>3</sub>O<sub>4</sub> thin film and suspension are quite similar to absorptions diminished beyond 700 nm [Fig. 3(a)]. The red-shift of the absorption peak in Fe<sub>3</sub>O<sub>4</sub>@Cu<sub>2-x</sub>S has been explained by the SPR coupling between the nanoparticles. [18,19] Tian et al. [9] pointed out that the NIR absorption can be attributed to the Cu<sub>2-x</sub>S shell.

The nanoparticle size dependence of absorption has been reported for the  $Fe_3O_4@Cu_{2-x}S$  solution. [9] The absorption peak shifts from 960 to 1150 nm as the  $Fe_3O_4@Cu_{2-x}S$  particle size increases from sub-10 to 15 nm. [9] Figures 3(b) and 3(c) show the TEM images of  $Fe_3O_4$  and  $Fe_3O_4@Cu_{2-x}S$  nanoparticles. As shown in this figure, the average size of  $Fe_3O_4$  is

around 10 nm, while that of  $Cu_{2-x}S$  coated nanoparticles is about 15 nm. This considerable size difference suggests the  $Cu_{2-x}S$  coating on the nanoparticles of  $Fe_3O_4$ , which is consistent with the report by Tian et al. [9]

The Raman experiments were carried out with 514 and 785 nm laser extinctions (Fig. 4). As shown in Fig. 4(a), the Fe<sub>3</sub>O<sub>4</sub> nanoparticles exhibit a small peak at 680 cm<sup>-1</sup> by 514 nm extinction, which is consistent with a previous report. [20] However, no obvious strong peaks are observed from the Fe<sub>3</sub>O<sub>4</sub>@Cu<sub>2-x</sub>S nanoparticles by 514 nm extinction [Fig. 4(b)]. Under 785 nm laser extinction, as shown in Fig. 4(a), there are no significant differences between Fe<sub>3</sub>O<sub>4</sub> and Fe<sub>3</sub>O<sub>4</sub>@Cu<sub>2-x</sub>S in Raman spectra.

# PT conversion efficiency, SAR, and *U*-factor

The PT conversion efficiency,  $\eta$ , is defined as the ratio of the thermal energy generated by the sample to the incident photon energy. The PT conversion efficiency for solar light

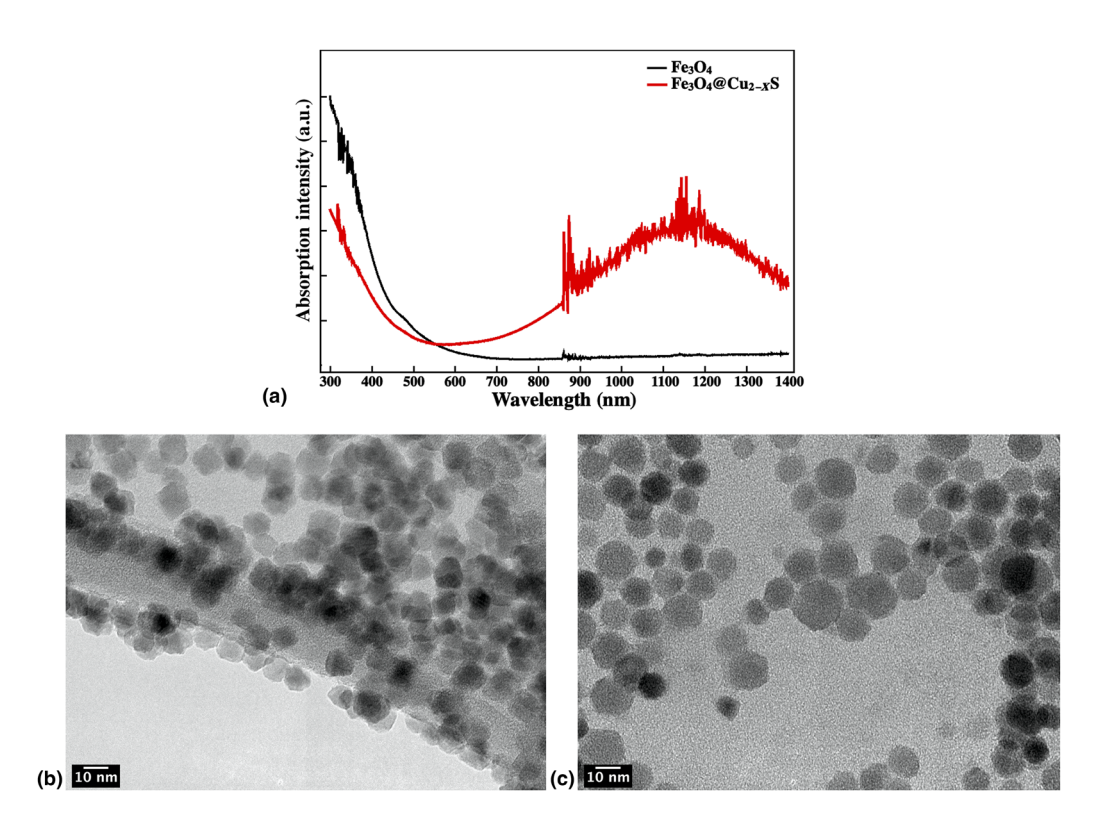


Figure 3. (a) Absorption spectra of the Fe<sub>3</sub>O<sub>4</sub> and Fe<sub>3</sub>O<sub>4</sub>@Cu<sub>2-x</sub>S solution (0.1 mg/mL). TEM images of (b) Fe<sub>3</sub>O<sub>4</sub> and (c) Fe<sub>3</sub>O<sub>4</sub>@Cu<sub>2-x</sub>S nanoparticles.

was developed by Jin et al. and given by the following equation<sup>[21]</sup>:

$$\eta = \frac{(C_{\text{glass}} m_{\text{glass}} + C_{\text{PT}_{\text{material}}} m_{\text{PT}_{\text{material}}} + C_{\text{polymer}} m_{\text{polymer}}) \Delta T_{\text{max}}}{IA \Delta t}$$

$$\approx \frac{C_{\text{glass}} m_{\text{glass}} \Delta T_{\text{max}}}{IA \Delta t} \tag{3}$$

where C is the specific heat capacity (J/g °C), m is mass (g),  $\Delta T_{\text{max}}$  is the maximum change in temperature increase of the

sample (°C), I is the power density (W/cm²), A is the surface area of the sample, and  $\Delta t$  is the time for sample to achieve the maximum temperature (s). In this research, the specific heat of glass is 0.84 J/g °C, and mass of the substrate is 1.75 g, the power density is 0.1 W/cm², and the surface area of the substrate is  $2.54 \times 2.54$  cm².

The specific absorption rate (SAR) of a PT material is a measure of the rate at which energy is absorbed by the material when exposed to incident light and can be expressed as follows<sup>[21]</sup>:

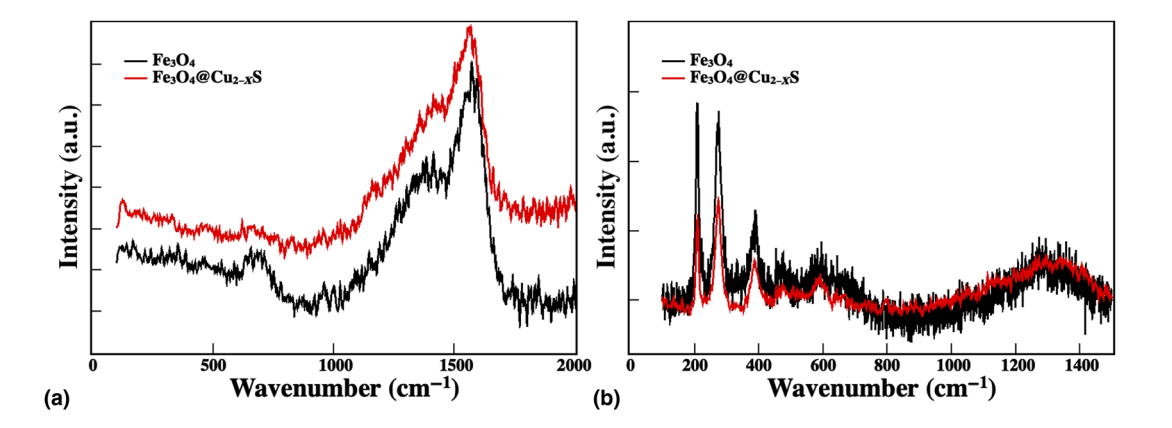


Figure 4. Raman spectra of  $Fe_3O_4$  and  $Fe_3O_4$ @ $Cu_{2-x}S$  on micro slides. (a) Raman spectra by 514 nm laser and (b) 785 nm laser excitations at room temperature.

$$SAR = \frac{(C_{glass} m_{glass} + C_{PT \, material} m_{PT \, material} + C_{polymer} m_{polymer}) \Delta T_{max} - (C_{glass} m_{glass} + C_{polymer} m_{polymer}) \Delta T_{control}}{m_{PT \, material} \Delta t}$$
(4)

where  $\Delta T_{\rm control}$  is the maximum change in temperature increase of the PMMA film without PT materials. This equation can be simplified as<sup>[22]</sup>:

$$SAR = \frac{C_{\text{glass}} m_{\text{glass}} (\Delta T_{\text{max}} - \Delta T_{\text{control}})}{m_{\text{PT material}} \Delta t}$$
 (5)

In accordance with ASTM C1199-14, [23] the *U*-factor can be expressed as follows:

$$U = \frac{1}{(1/h_{\rm h}) + (1/h_{\rm c}) + (1/U_{\rm L})}$$
 (6)

we have

$$\frac{1}{U_{\rm I}} = \frac{1}{h_{\rm h}} \times \frac{(T_{\rm g} - T_{\rm out})}{(T_{\rm in} - T_{\rm g})} \tag{11}$$

and

$$\frac{1}{h_{\rm h}} + \frac{1}{U_{\rm L}} = \frac{1}{h_{\rm h}} \times \frac{(T_{\rm in} - T_{\rm out})}{(T_{\rm in} - T_{\rm g})}$$
(12)

The *U*-value or *U*-factor is a measure of how much heat loss through a window, which is also known as the thermal transmittance. The *U*-factor equation can be expressed as follows<sup>[22]</sup>:

$$U = \frac{1}{\left(\frac{T_{\rm in} - T_{\rm out}}{T_{\rm in} - T_{\rm g}}\right) \times \frac{1}{1.46 \times \left[\frac{(T_{\rm in} - T_{\rm g})}{L}\right]^{0.25} + \sigma e \left[\frac{(T_{\rm in}^4 - T_{\rm g}^4)}{(T_{\rm in} - T_{\rm g})}\right]} + \frac{1}{\sqrt{(0.84 \times (T_{\rm g} - T_{\rm out})^{1/3})^2 + (2.38 \times v^{0.89})^2}}$$
(13)

where  $h_h$  and  $h_c$  are, respectively, the interior and exterior heat coefficients, and  $U_L$  is the heat transfer coefficient of the window pane.  $h_h$  and  $h_c$  are respectively expressed as follows:

$$h_{\rm h} = 1.46 \times \left[ \frac{(T_{\rm in} - T_{\rm g})}{L} \right]^{0.25} + \sigma e \left[ \frac{(T_{\rm in}^4 - T_{\rm g}^4)}{(T_{\rm in} - T_{\rm g})} \right]$$
 (7)

$$h_{\rm c} = \sqrt{(0.84 \times (T_{\rm g} - T_{\rm out})^{1/3})^2 + (2.38 \times v^{0.89})^2}$$
 (8)

where  $T_{\rm in}$  is the interior room temperature,  $T_{\rm out}$  is the exterior window temperature, v is wind speed, L is the height of the window,  $\sigma$  is Stefan–Boltzmann constant (5.67 × 10<sup>-8</sup> W/m<sup>2</sup> K<sup>4</sup>), e is emissivity, and  $T_{\rm g}$  is the original interior window temperature.

Neglecting the edge and radiation effects,  $U_{\rm L}$  can be derived as follows:

Heat loss via the window assembly

$$= U_{\rm L} \times A \times (T_{\rm g} - T_{\rm out}) \tag{9}$$

Heat loss from the room to the interior window

$$= h_{\rm h} \times A \times (T_{\rm in} - T_{\rm g}) \tag{10}$$

Since these two heat loss rates must be equaled:

$$U_{\rm L} \times A \times (T_{\rm g} - T_{\rm in}) = h_{\rm h} \times A \times (T_{\rm in} - T_{\rm g})$$

The calculation parameters of the *U*-factor are obtained from NFRC 100-2017<sup>[3]</sup>:  $T_{\rm in}$  is 21.11 °C (294.26 K);  $T_{\rm out}$  is -17.78 °C (255.37 K); v is 5.50 m/s; L is 1.499 m, and e is 0.84 in this study. Assuming the original interior window temperature is 5 °C, and  $T_{\rm g}$  is calculated to be 278.15 K +  $\Delta T_{\rm max}$ .

The PT conversion efficiency, SAR, and U-factor of each sample are calculated by using above equations and the results are summarized in Table I. For a given AVT, the Fe<sub>3</sub>O<sub>4</sub>@Cu<sub>2-x</sub>S thin film is shown to have a higher PT conversion efficiency than that of the Fe<sub>3</sub>O<sub>4</sub> thin film due to pronounced NIR absorption of the former. One can see that the *U*-factor decreases from 2.21 to 1.54 W/m<sup>2</sup> K by increasing the mass of Fe<sub>3</sub>O<sub>4</sub> nanoparticles in the thin-film samples. The U-factor is reduced more significantly from 2.21 to 1.46 W/ m<sup>2</sup> K with increasing mass of Fe<sub>3</sub>O<sub>4</sub>@Cu<sub>2-x</sub>S. According to Energy Star certification in the USA, the Department of Energy (DOE) general requirement of U-factor for the window is  $\leq 1.7 \text{ W/m}^2 \text{ K} (0.3 \text{ Btu/h ft}^2 \,^{\circ}\text{F}).^{[24]}$  The best *U*-values for different materials are 1.54 W/m<sup>2</sup> K (F-1) and 1.46 W/m<sup>2</sup> K (FC-1) in this research, these values are less than the minimum requirement of DOE for windows (1.7 W/m<sup>2</sup> K). Consequently, we claim that the best U-values are well below the DOE requirement for windows. Although some of the U-factors are satisfactory for commercial windows, most of them are double panes for cold climate regions. The low U-factors obtained in this study are from the single-layer coating on a glass substrate, therefore qualified for the single-pane design.

As shown in Table I, for the Fe<sub>3</sub>O<sub>4</sub> films, SAR consistently decreases with increasing concentration. In contrast, the SAR of Fe<sub>3</sub>O<sub>4</sub>@Cu<sub>2-x</sub>S shows rather random values which are not affected by a change in concentration. This difference may



**Table I.** Parameters in the calculation used and results of  $Fe_3O_4$  and  $Fe_3O_4$ @ $Cu_{2-x}S$  thin films under simulated solar irradiation (0.1 W/cm<sup>2</sup>).

	$ ho_{ m pm}~( imes 10^{-4}~{ m g/cm^2})$	$\Delta T_{max}$ (°C)	AVT (%)	η (%)	SAR (W/g)	<i>U</i> (W/m <sup>2</sup> K)
F-1	4.57	6.53	64.8	2.56	1.88	1.54
F-2	4.07	5.80	70.4	2.27	1.80	1.65
F-3	3.55	4.93	75.2	1.93	1.64	1.77
F-4	2.54	3.90	80.4	1.53	1.58	1.91
F-5	1.52	2.40	85.1	0.94	0.92	2.11
FC-1	5.08	7.10	65.2	2.78	1.89	1.46
FC-2	4.07	5.93	69.7	2.33	1.86	1.63
FC-3	2.54	5.43	74.9	2.13	2.64	1.70
FC-4	2.03	4.63	80.5	1.82	2.62	1.81
FC-5	1.01	2.73	85.0	1.07	1.95	2.07
Control	0	1.60	91.0	N/A	N/A	2.21

The F and FC are initialisms of Fe<sub>3</sub>O<sub>4</sub> and Fe<sub>3</sub>O<sub>4</sub>@Cu<sub>2-x</sub>S. The PT material area density on the glass,  $\rho_{pm}$ , represents the mass of thin film per coating area (g/cm<sup>2</sup>),  $\Delta T_{max}$  is the maximum steady temperature difference of the sample, U is the heat transfer coefficient (W/m<sup>2</sup> K), and  $\eta$  is the PT conversion efficiency.

attribute to large NIR absorptions by the  $Fe_3O_4@Cu_{2-x}S$  films rendering the materials with more light absorptions that are less dependent on concentration.

It is interesting to note that both sample F-2 (Fe<sub>3</sub>O<sub>4</sub>) and FC-2 (Fe<sub>3</sub>O<sub>4</sub>@Cu<sub>2-x</sub>S) have the same area density (4.07 ×  $10^{-4}$  g/cm<sup>2</sup>). As expected, Fe<sub>3</sub>O<sub>4</sub>@Cu<sub>2-x</sub>S film (FC-2) shows better performance with greater PT respond ( $\Delta T_{\rm max}$ ), higher PT conversion efficiency ( $\eta$ ), and lower *U*-factor, all attributable to the large NIR absorptions in this compound.

#### **Conclusions**

We conclude in this study that it is possible to reduce thermal transmittance of building skin via a new concept of OTI without relying on any intervening medium. This novel approach fundamentally lifts the limiting barrier of the physical thermal insulators and paves a new way for single-pane designs via OTI. OTI requires a "U"-shaped spectrum with strong UV and NIR absorptions but enhanced visible transmittance, based on which new materials can be designed with spectral selectivity and tunability. To reduce thermal transmittance, a PT coating can be applied on single-pane window surfaces. Upon solar irradiation, the temperature of the PT coating can be significantly increased, reducing the temperature difference between the window inner surface and the room interior, leading to lowered U-factor. The proof of concept is successfully demonstrated on two materials systems, namely Fe<sub>3</sub>O<sub>4</sub> and Fe<sub>3</sub>O<sub>4</sub>@Cu<sub>2-x</sub>S, both are highly PT but with different absorption spectra. While the former is with strong UV absorption, the latter is characterized with both UV and NIR absorptions exhibiting a typical "U"-shape, therefore making this system an ideal candidate for single-pane applications. Due to pronounced NIR absorption of Fe<sub>3</sub>O<sub>4</sub>@Cu<sub>2-x</sub>S, its overall performance is significantly improved over Fe<sub>3</sub>O<sub>4</sub>, supported by the data of the PT effect ( $\Delta T_{\text{max}}$ ), PT conversion efficiency ( $\eta$ ), and *U*-factor. Furthermore, two opposing factors: concentration and AVT were studied and optimized providing a new base for engineering design of single panes.

# **Acknowledgments**

This research is supported by the National Science Foundation CMMI-1635089. We thank Dr. Vasseline Shanov for using the Raman spectrometer and Dr. Andrew J. Steckl for the Perkin-Elmer spectrophotometer.

#### **References**

- U.S. Energy Information Administration: United States: International Energy Outlook 2019 with projections to 2050, 2019.
- ARPA-E: Single-pane highly insulating efficient lucid designs (SHIELD) program overview, 2014.
- National Fenestration Rating Council Incorporated: ANSI/NFRC 100-2017 [E0A2]: procedure for determining fenestration product U-factors. National Fenestration Rating Council Incorporated, July 18, 2018.
- ASTM G173-03: Standard tables for reference solar spectral irradiances: direct normal and hemispherical on 37° tilted surface. ASTM International: West Conshohocken, PA, 2012. http://www.astm.org/cgibin/resolver.cgi?G173
- X. Huang, I.H. El-Sayed, W. Qian, and M.A. El-Sayed: Cancer cell imaging and photothermal therapy in the near-infrared region by using gold nanorods. J. Am. Chem. Soc. 128, 2115–2120 (2006).
- L. Feng, L. Wu, and X. Qu: New horizons for diagnostics and therapeutic applications of graphene and graphene oxide. *Adv. Mater.* 25, 168–186 (2013).
- D. Shi, M.E. Sadat, A.W. Dunn, and D.B. Mast: Photo-fluorescent and magnetic properties of iron oxide nanoparticles for biomedical applications. *Nanoscale* 7, 8209–8232 (2015).

- M. Chu, Y. Shao, J. Peng, X. Dai, H. Li, Q. Wu, and D. Shi: Near-infrared laser light mediated cancer therapy by photothermal effect of Fe<sub>3</sub>O<sub>4</sub> magnetic nanoparticles. *Biomaterials* 34, 4078–4088 (2013).
- Q. Tian, J. Hu, Y. Zhu, R. Zou, Z. Chen, S. Yang, R. Li, Q. Su, Y. Han, and X. Liu: Sub-10 nm Fe<sub>3</sub>O<sub>4</sub>@Cu<sub>2-x</sub>S core-shell nanoparticles for dualmodal imaging and photothermal therapy. *J. Am. Chem. Soc.* 135, 8571–8577 (2013).
- R. Zhao, X. Sun, J. Sun, L. Wang, and J. Han: Polypyrrole-modified CuS nanoprisms for efficient near-infrared photothermal therapy. *RSC Adv.* 7, 10143–10149 (2017).
- M.A. Zaitoun, W.R. Mason, and C.-T. Lin: Magnetic circular dichroism spectra for colloidal gold nanoparticles in xerogels at 5.5 K. J. Phys. Chem. B 105, 6780–6784 (2001).
- J.S. Melinger, V.D. Kleiman, D. McMorrow, F. Gröhn, B.J. Bauer, and E. Amis: Ultrafast dynamics of gold-based nanocomposite materials. *J. Phys. Chem. A* 107, 3424–3431 (2013).
- Y. Zhao, M.E. Sadat, A.W. Dunn, H. Xu, C.-H. Chen, W. Nakasuga, R.C. Ewing, and D. Shi: Photothermal effect on Fe<sub>3</sub>O<sub>4</sub> nanoparticles irradiated by white-light for energy-efficient window applications. *Solar Energy Mater. Solar Cells* 161, 247–254 (2017).
- T. Wei, Y. Liu, W. Dong, Y. Zhang, C. Huang, Y. Sun, X. Chen, and N. Dai: Surface-dependent localized surface plasmon resonances in CuS nanodisks. ACS Appl. Mater. Interfaces 5, 10473–10477 (2013).
- M. Shabaninezhad and G. Ramakrishna: Theoretical investigation of size, shape, and aspect ratio effect on the LSPR sensitivity of hollow-gold nanoshells. J. Chem. Phys. 150, 144116 (2019).
- 16. M.E. Sadat, M.K. Baghbador, A.W. Dunn, H.P. Wagner, R. Ewing, J. Zhang, H. Xu, G. Pauletti, D. Mast, and D. Shi: Photoluminescence and photothermal effect of Fe<sub>3</sub>O<sub>4</sub> nanoparticles for medical imaging and therapy. *Appl. Phys. Lett.* 105, 091903 (2014).
- K. Jiang, D.A. Smith, and A. Pinchuk: Size-dependent photothermal conversion efficiencies of plasmonically heated gold nanoparticles. *J. Phys. Chem. C* 117, 27073–27080 (2013).
- M. Kanehara, H. Koike, T. Yoshinaga, and T. Teranishi: Indium tin oxide nanoparticles with compositionally tunable surface plasmon resonance frequencies in the near-IR region. *J. Am. Chem. Soc.* 131, 17736– 17737 (2009).
- J.B. Lassiter, J. Aizpurua, L. Hernandez, D. Brandl, I. Romero, S. Lal, J. Hafner, P. Nordlarder, and N. Halas: Close encounters between two nanoshells. *Nano Lett.* 8, 1212–1218 (2008).
- D. De Faria, S. Venâncio Silva, and M.T. De Oliveira: Raman microspectroscopy of some iron oxides and oxyhydroxides. *J. Raman Spectrosc.* 28, 873–878 (1997).
- 21. H. Jin, G. Lin, L. Bai, M. Amjad, E.P. Bandarra Filho, and D. Wen: Photothermal conversion efficiency of nanofluids: an experimental and numerical study. *Solar Energy* 139, 278–289 (2016).
- Y. Zhao, A. Dunn, and D. Shi: Effective reduction of building heat loss without insulation materials via the photothermal effect of a chlorophyll thin film coated "Green Window". MRS Commun. 9, 675–681 (2019).
- 23. ASTM C1199-14: Standard test method for measuring the steady-state thermal transmittance of fenestration systems using hot box methods. ASTM International: West Conshohocken, PA, 2014. www.astm.org
- 24. ENERGY STAR Program Requirements for Residential Windows, Doors, and Skylights: https://www.energystar.gov/products/building\_products/residential\_windows\_doors\_and\_skylights/key\_product\_criteria#performanceCriteria (accessed October 31, 2019).